CMOS 3-AXIS ACCELEROMETERS WITH INTEGRATED AMPLIFIER

E. J. J. Kruglick, B. A. Warneke, and K. S. J. Pister

Berkeley Sensor and Actuator Center
University of California, Berkeley
497 Cory Hall, Berkeley, CA 94720, USA

ABSTRACT

Design, fabrication, and testing of multi-axis CMOS piezoresistive accelerometers is described. Vertical axis accelerometers have been fabricated in multiple processes using a production tested maskless bulk etch step. Horizontal axis accelerometers have also been fabricated and require an additional assembly step. Acceleration sensing in based on the piezoresistive behavior of the gate polysilicon in standard CMOS. Integrated amplifiers were designed and built on chip and have been characterized. Characterization is also presented for sensitivity, angular response, frequency response, axis of maximum sensitivity, temperature coefficient of offset, and temperature coefficient of sensitivity. Results are presented for a single chip with integrated full three axis acceleration sensing.

INTRODUCTION

Micromachined accelerometers are not new. Many groups have made them based on a wide variety of sensing mechanism, among them capacitance [1][2][3][4][5], piezoresistance [6][7], and electron tunneling[8]. Micromachined accelerometers have also been successful as commercial products for several companies, such as Analog Devices, Motorola, and IC Sensors. For a new accelerometer technology to be attractive it must be low cost, reliable, and perform well.

The design presented here uses a standard CMOS process. Thus it can be fabricated without the cost of a custom process and can be integrated monolithically with electronics to reduce chip count and wire bonding. TSMC foundry is currently offering 6 inch wafers of 0.5μm CMOS for US$600, resulting in a price of about US$0.05 per square millimeter. Adding an accelerometer to an existing ASIC design costs just pennies for die area. However, packaging and testing costs often dominate.

DEVICE CONCEPT AND TECHNOLOGY

The piezoresistivity of LPCVD deposited polysilicon is a well understood and characterized phenomenon[9]. Gauge factor can be estimated from doping levels and in standard CMOS fabrication we expect it to be about -20.

This piezoresistivity is used to sense the strain induced in the legs of a suspended accelerometer structure (Figs. I and II). Figure I shows a diagram of the basic design.

The proof mass is made of all the available layers, in a typical two metal process this might be three dielectrics, two metals, and a polysilicon layer. The hinges carry the signal back to the chip if the structure is bent up (and would be omitted for the vertical axis). The piezoresistor is placed at the point of maximum strain (once the hinges are locked upright). The strain is proportional to

 0-7803-4412-X/98/$10.00 © 1998 IEEE

Authorized licensed use limited to: Univ of Calif Berkeley. Downloaded on October 23,2022 at 23:26:37 UTC from IEEE Xplore. Restrictions apply.

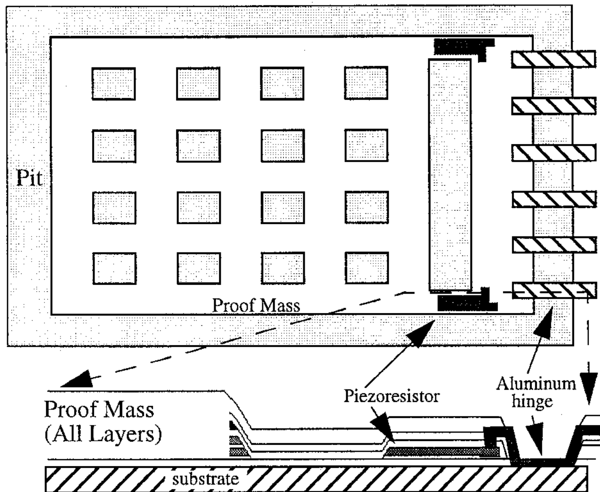

Fig. I: Overview of accelerometer design. Can be made with or without hinges. Motion is in and out of the page in top diagram, up and down in bottom diagram.

structural displacement, which is proportional to acceleration. The structure shown in figure II, for example, experiences a measured resistance change factor of 1.25×10^{-5} per gravity(G) of acceleration. The sense and reference structures are hooked up in series to form a half bridge. For this device the support beams are 40μm wide and 90μm long with the piezoresistor occupying the first 30μm, the mass is approximately 14.3ng and the piezoresistor is 0.95μm from the neutral axis of the support beam. Using these numbers and the nominal thicknesses for this particular process we get an expected resistance change factor approximately twice the experimental value above. Closer estimation may require finer modeling such as FEM.

The structure in figure I is supported only on one side to reduce problems with residual stress. Even with a singly supported structure local regions such as the support arms can become clamped-clamped during release if not designed carefully. Strain resulting from residual stress can buckle or shatter a clamped-clamped structure during release. This has been observed on numerous structures. We have fabricated some accelerometer structures anchored at all four corners by implementing strain-absorbing curves in the design of the support legs, but due to a design flaw these did not prove testable.

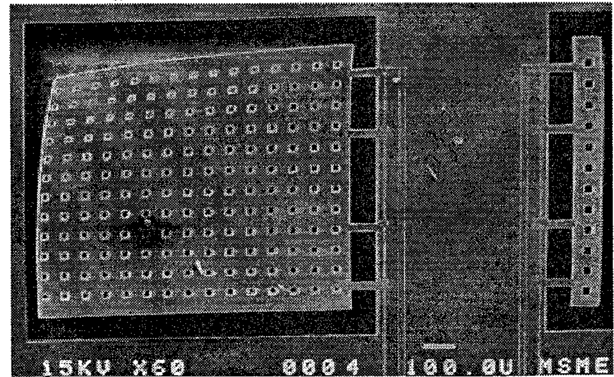

Fig. II: SEM of Z-axis accelerometer with reference structure. Curl in upper left is charge induced.

The structure holding the reference resistors (in essence a small accelerometer itself) was used to equalize the release of residual stress on the reference resistors. Residual stress differences have been observed in the past to dramatically affect sensing. The reference structure also provides a similar thermal environment for both resistors, this minimizes the number of contributors to temperature drift.

Fabrication of the structure is shown shematically in Fig. III. After finishing the standard CMOS fabrication process the devices are exposed to a xenon difluoride etch [11] to sacrificially etch the substrate and release the accelerometers. This etch does not damage electronics. A commercial CMOS wafer exposed to xenon difluoride showed no degradation in yield or performance, even after accelerated aging tests. After the xenon difluoride etch the devices are packaged, wirebonded, and tested. If non-outgassing adhesives are used the accelerometers can be packaged before xenon difluoride etching to ease pick and place requirements. Of the 12 die etched and packaged so far all 12 have been functional.

Out of plane sensors for the two horizontal axes are made using aluminum hinges and locking structures[10]

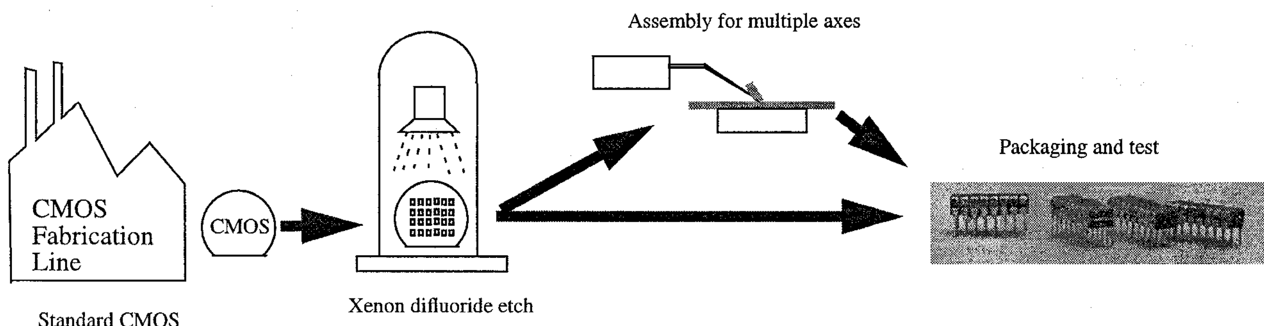

Fig. III: Fabrication flow for integrated accelerometers, with and without assembly for out of plane sensors.

Authorized licensed use limited to: Univ of Calif Berkeley. Downloaded on October 23,2022 at 23:26:37 UTC from IEEE Xplore. Restrictions apply.

(figure X). Assembly of these is done using micromanipulators.

SINGLE (Z) AXIS CHARACTERIZATION

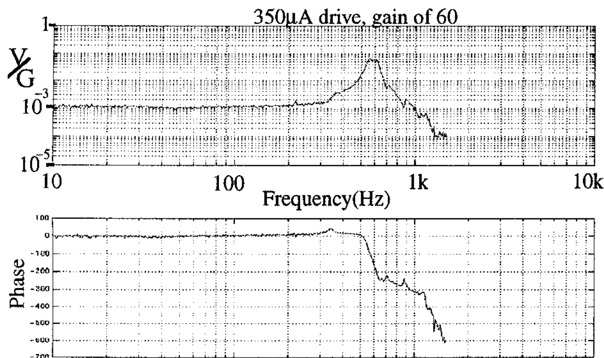

Fig. IV: Typical magnitude and phase response for accelerometer shown in figure I at atmospheric pressure

Figure IV shows a typical magnitude and phase plot for output from the accelerometer shown in figure II for a vertically applied acceleration. The resonant frequency can be seen to be about 600Hz and the Q factor about 60. For all acceleration tests, unless otherwise mentioned, the acceleration was supplied by a Brüel & Kjær PM Vibration Exciter Type 4808 and a Brüel & Kjær 4381 with individual factory characterization was used as a reference accelerometer.

Figure V shows the assumed first mode for calculation of the resonant frequency. Because most of the bending takes place in the support beam, rotational energy in the proof mass resonance must be taken into account. Using the Raleigh condition for equal maximum potential and kinetic energy on this mode leads to:

$$\omega = \sqrt{\frac{k_\Theta}{J + mr^2}} \quad \textbf{(EQ 1)}$$

where the variables are labelled in figure V. Applying the calculated spring constant of the support beams and the estimated mass and moment of the structure this method

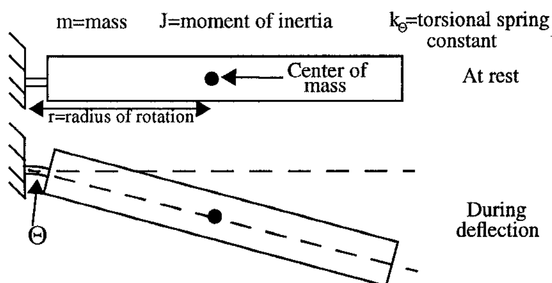

Fig. V: Bending mode used for Ralegh analysis of resonant frequency. Rotational energy must be taken into account.

estimates a resonant frequency of 740Hz. The observed resonant frequency in figure IV is 600Hz. The difference may be due to unmodeled compliance of the undercut support anchors.

The responsivity is 1.25×10^{-5} per gravity. The sense resistor in the device in figure I is 4kΩ, leading to a resistance change of.05Ω per gravity. For test the device was wired with a constant current circuit driving 350µA, resulting in a signal of 17.5mV per gravity raw output response. This can be compared to the thermal noise in the sense resistor of $16\text{nV}/\sqrt{Hz}$. The CMOS amplifier shown in figure X has a measured broadband noise floor of $30\text{nV}/\sqrt{Hz}$. Absent the 1/f noise discussed below, the minimum resolution is established by the sum of the noise in the resistors and amplifier as $38\text{nV}/\sqrt{Hz}$ and the theoretical sensitivity limit at this current is $2.2\mu\text{G}/\sqrt{Hz}$. It is typical to cite product performance limits for commercial accelerometers at the 7σ level the minimum reliable detection threshold is $15.2\mu\text{G}/\sqrt{Hz}$ or 0.3mG over a 500Hz bandwidth. Performance improves roughly linearly with increased current. The devices have been driven with several milliamps for several days with no performance degradation.

Another important consideration is the axis of maximum sensitivity. In order to measure this, a mounting jig was built in which the accelerometer could be shaken in various positions of roll and pitch. A response surface was taken (figure VI) with intervals of 10° from -150° to 110° in pitch and from -130° to 150° in roll. The remaining 80° by 100° solid angle could not be explored due to

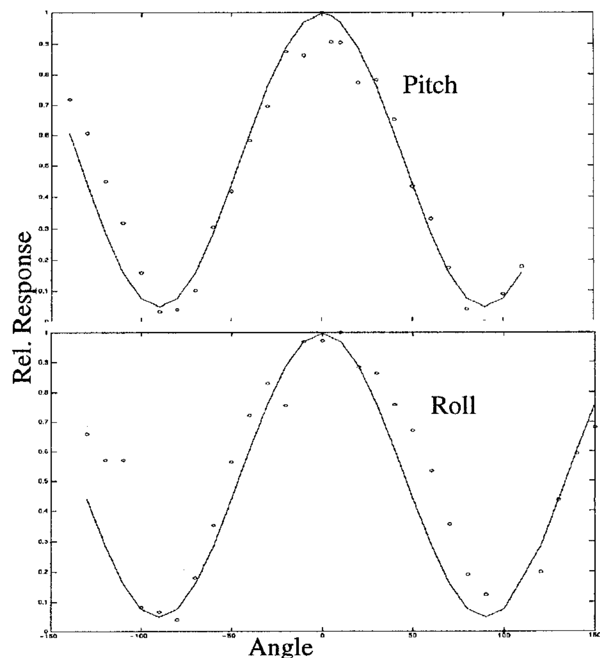

Fig. VI: Packaged and mounted accelerometer response versus angle of acceleration. Solid lines represent fitted sine wave for no cross axis component.

Authorized licensed use limited to: Univ of Calif Berkeley. Downloaded on October 23,2022 at 23:26:37 UTC from IEEE Xplore. Restrictions apply.

mechanical limits of the testing jig but the data exhibits symmetry so this is thought not to have impacted the validity of the experiment. Figure VI shows angular response characterization for both pitch and roll along with a fitted sine wave for perfect cross axis isolation as a solid line. The scatter in the points is somewhat high because the data was taken at low amplitude. This limitation was due to the low accelerations possible with the rotating jig (Fig VII) loading the shaker. Testing was done with signals at 100Hz to avoid drift since a temperature signal was not available to do correction. A statistical least squares fit was performed between the normalized expected output (shown in figure VI as a solid line of semi-arbitrary magnitude) and the data, yielding the "axis of sensitivity." The standard deviation on this measurement-fit-estimate was 5°. The estimate was -5° pitch, -5° roll, which is within one standard deviation of zero.

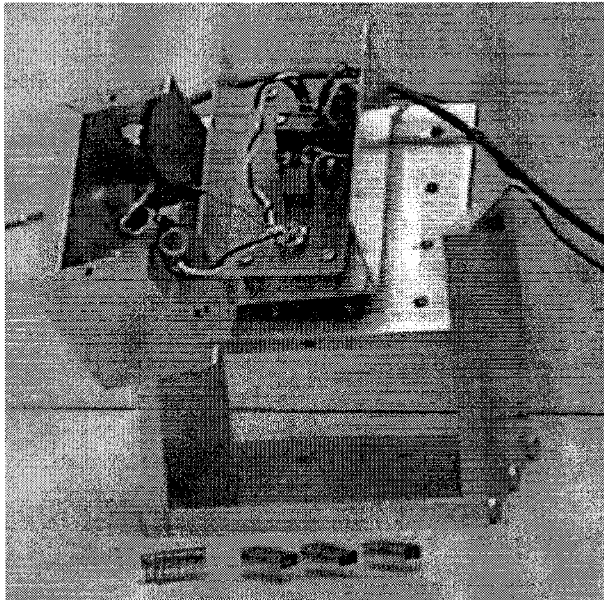

Fig VII: Rotating shaker jig and several packaged, functional CMOS accelerometers. Coaxial output from shielded box is on left, power and temperature signal are on right. Temperature sensor is connected to accelerometer with thermally conductive tape.

Temperature characterization of the accelerometer was performed with the sensor both upright and inverted while cycling ambient temperature. A solid state temperature sensor was mounted to the accelerometer package during testing using thermal adhesive transfer tape and the resulting data was fitted for temperature coefficient. This yielded coefficients of temperature with +1 gravity or -1 gravity applied, from which temperature coefficient of offset and temperature coefficient of sensitivity could be derived. Validity of this test requires that the true sensitive axis be known. Across several accelerometers the voltage offset with temperature varied only slightly from 0.32mV/C° to 0.40mV/C°. The temperature dependence of sensitivity had a mean of 3.8μV/GC° and standard deviating of 5.5μV/GC° on multiple accelerometers with constant current of 625μA. The offset with temperature and sensitivity change with temperature were also analytically considered with respect to resistor mismatch. The analytic equations yield a good estimate of the voltage offset with temperature using statistical mismatch data from the process in question. The analytic prediction of the sensitivity change with temperature, however, does not match well. Equations taking into account the temperature coefficient of gauge factor [12] are being explored. Temperature compensation leads to significant drift reduction, even without the temperature sensor being integrated with the accelerometer (Fig. VIII).

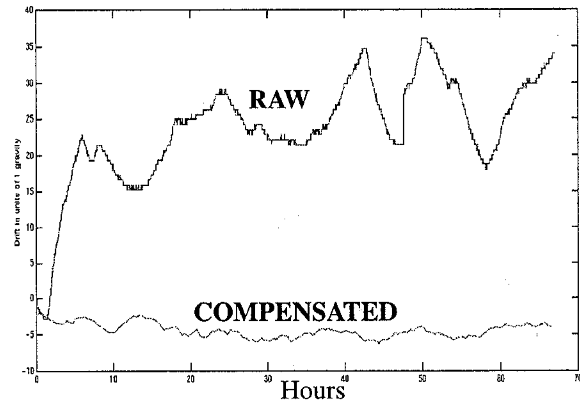

Fig. VIII: Long term behavior of the accelerometer, with and without temperature compensation.

MULTI-AXIS ACCELEROMETERS

As stated earlier, the accelerometers for other than the vertical axis are folded upward out of the plane on aluminum hinges as in [10]. The result is a vertical version of the accelerometer seen in figure I. A close-up of the hinges and a locking structure to provide rigidity is shown in figure IX. Reference resistors are located on the rotated structure because thermal dissipation of a microresistor in air depends substantially on orientation [13]

Linearity characterization results are shown in figure X for both a fixed z-axis accelerometer and a rotated x-axis

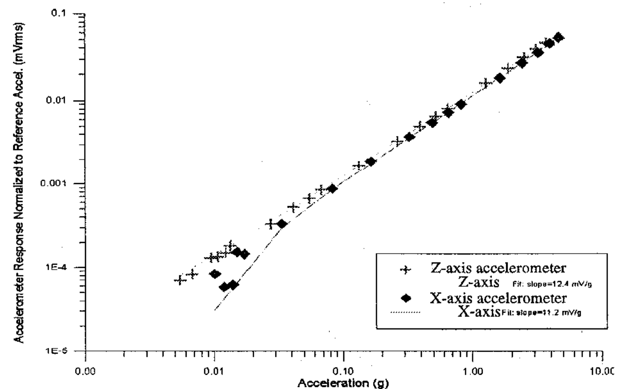

Fig. X: Z-axis and X-axis accelerometer response showing linearity over 3 orders of magnitude.

Authorized licensed use limited to: Univ of Calif Berkeley. Downloaded on October 23,2022 at 23:26:37 UTC from IEEE Xplore. Restrictions apply.

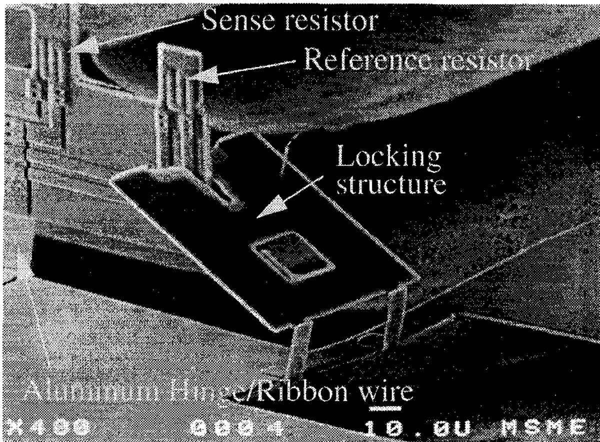

Fig IX: Closeup of hinged section of assembled accelerometer. Aluminnum hinges also act as electrical connection. Wire traces and piezoresistors are visible on structure. Locking device reduces undesirable flexing.

accelerometer. The results were gathered over three orders of magnitude at 100Hz. It can be seen that the accelerometer which has been folded out of the plane on hinges has slightly different response characteristics at extremely low accelerations. This is still under investigation.

On and off axis sensitivity must again be characterized for the out of plane structure and is shown in figure XI. On and off axis sensitivity is shown for both a flat and assembled accelerometer. More z-axis data is presented because this device was fabricated in a different process than the z-axis data previously shown. The rotated accelerometers and their accompanying flat counterparts were fabricated in the ORBIT 2μm CMOS line through the MOSIS foundry service, the earlier device was manufactured in a proprietary industrial BiCMOS process. Both use similar designs and have similar performance, showing the process portability of this approach.

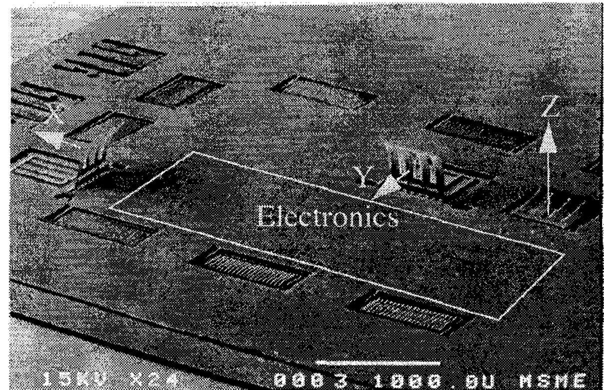

Fig. XII: Three accelerometer axes with integrated amplifiers together on one die.

It can be seen here that cross axis isolation, while not ideal, is certainly good enough to permit signal processing to determine the true acceleration axis.

Figure XII shows a CMOS chip with three orthogonal integrated accelerometers with on chip electronics. The intent was to use the integrated amplifiers as preamplification stages. They were designed without flicker noise coefficients because none were available for the foundry. Upon receiving the devices the noise was characterized by matching to simulation (figure XIII) [14], and the corner frequency was found to be 9kHz. Given that the signals of interest all lie below 1kHz this is quite inconvenient and gives a noise floor through these amplifiers of almost 3G from 0.5Hz to 500Hz.

A new chopper stabilized amplifier system with onboard temperature sensing is in fabrication.

CONCLUSION

CMOS multi-axis microaccelerometers have been built integrated on chip monolithically with electronics using a single maskless post processing step. Experimental

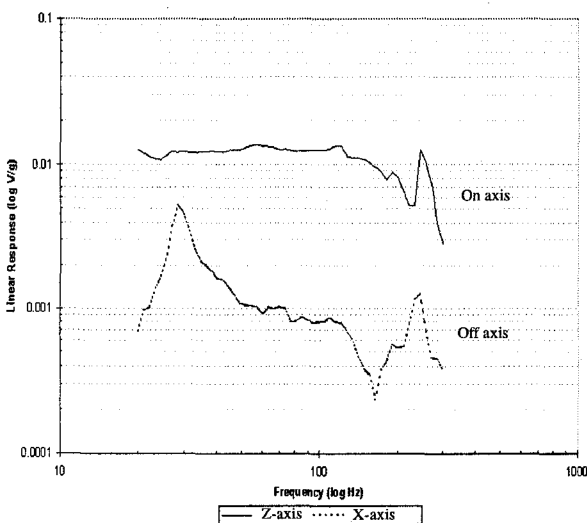

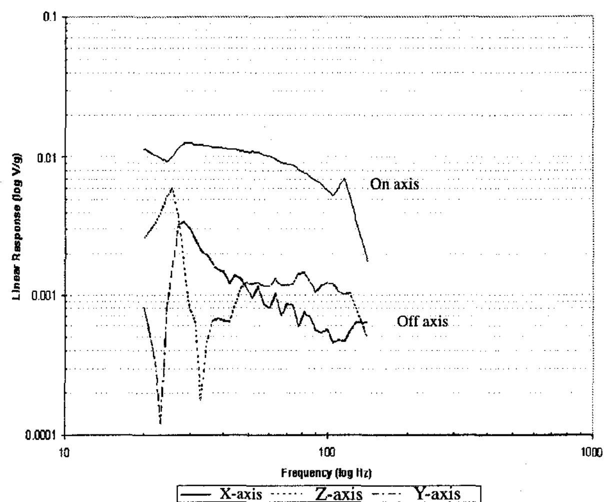

Fig. XI: On and off axis sensitivity and frequency response for multiple accelerometer axes on a single chip.

Authorized licensed use limited to: Univ of Calif Berkeley. Downloaded on October 23,2022 at 23:26:37 UTC from IEEE Xplore. Restrictions apply.

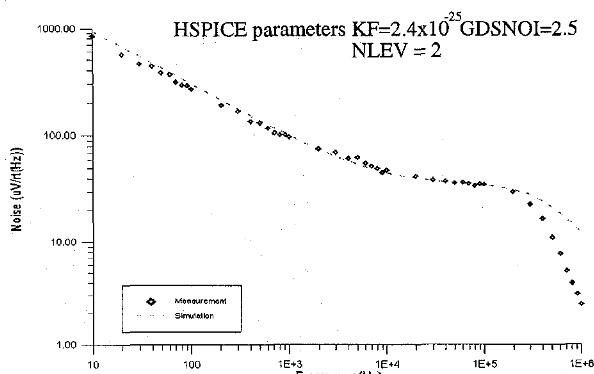

Fig. XIII: Measured amplifier output noise and fitted SPICE parameters. Voltage gain is 1000.

results show good cross axis sensitivity isolation, predictable and correctable temperature offset, and robustness of design with different standard CMOS process implementations.

ACKNOWLEDGEMENTS

We wish to acknowledge Ron Wilson for his skilled SEM work. Post processing fabrication work was done at the UCLA Nanofabrication facility and the UCB Microfabrication Laboratory. Additional support for this work came from the John and Fannie Mae Hertz Foundation and the Howard Hughes Doctoral Fellowship.

REFERENCES

[1] Greenwood, J.C. "A silicon bulk micromachined capacitive force feedback accelerometer", IEE Colloquium on Silicon Fabricated Inertial Instruments; London, UK: IEE, 1996. p.61-2. 50 pp.

[2] Selvakumar, A.; Ayazi, F.; Najafi, K. "A high sensitivity z-axis torsional silicon accelerometer", International Electron Devices Meeting Technical Digest; San Francisco, CA, USA, 8-11 Dec. 1996 p.765-8

[3] Smith, T.; Nys, O.; Chevroulet, M.; DeCoulon, Y.; Degrauwe, M. "A 15 b electromechanical sigma-delta converter for acceleration measurements", 1994 Proceedings of IEEE International Solid-State Circuits Conference - ISSCC '94, San Francisco, CA, USA, 16-18 Feb. 1994 p.160-1

[4] Lemkin, M.A.; Ortiz, M.A.; Wongkomet, N.; Boser, B.E.; Smith, J.H. "A 3-axis surface micromachined Sigma Delta accelerometer" 1997 IEEE International Solid-State Circuits Conference. Digest of Technical Papers, ISSCC; San Francisco, CA, USA, 6-8 Feb. 1997 p.202-3

[5] Hierold, C.; Hildebrandt, A.; Naher, U.; Scheiter, T.; Mensching, B.; Steger, M.; Tielert, R. "A pure CMOS surface-micromachined integrated accelerometer" Sensors and Actuators A (Physical), vol.A57, (no.2), p.111-16.

[6] Hong Chen; Minhang Bao; Haijun Zhu; Shaoqun Shen "A piezoresistive accelerometer with a novel vertical beam structure" Sensors and Actuators A (Physical), vol.A63, (no.1), Elsevier, Sept. 1997. p.19-25

[7] de Bruin, D.W.; Dunbar, M.L. "Smart sensors for acceleration measurement using a two chip approach"; Proceedings 7th International Conference for Sensors Transducers and Systems (SENSOR 95), Germany, 1995 Wunstorf-Steinhude, Germany: ACS Organisations GmbH, 1995. p.207-12

[8] Rockstad, H.K.; Reynolds, J.K.; Tang, T.K.; Kenny, T.W.; Kaiser, W.J.; Gabrielson, T.B. A miniature, high-sensitivity, electron tunneling accelerometer" 8th International Conference on Solid-State Sensors and Actuators and Eurosensors IX. (vol.2)- TRANSDUCERS '95, Stockholm, Sweden, 25-29 June 1995 p.675-8

[9] Mosser, V.; Suski, J.; Goss, J.; Obermeier, E. "Piezoresistive pressure sensors based on polycrystalline silicon" Sensors and Actuators A (Physical), vol.A28, (no.2), July 1991. p.113-32.

[10] Hoffman, E.; Warneke, B.; Kruglick, E.; Weigold, J.; Pister, K.S.J. "3D structures with piezoresistive sensors in standard CMOS" Proceedings IEEE Micro Electro Mechanical Systems 1995, Amsterdam, Netherlands, 29 Jan.-2 Feb. p.288-93

[11] Chu, P.B.; J.T. Chen; R. Yeh; G. Lin; J.C.P. Huang; B.A. Warneke; K.S.J. Pister "Controlled Pulse-Etching with Xenon Difluoride"; 1997 International Conference on Solid State Sensors and Actuators - TRANSDUCERS '97, Chicago, USA, June 16-19, p. 665-668

[12] Schafer, H.; Graeger, V.; Kobs, R. "Temperature-independent pressure sensors using polycrystalline silicon strain guages"; Sensors and Actuators, vol. 17, (no. 3-4) May 1989 p.521-7

[13] Gisela Lin, unpublished data on CMOS thermal actuators

[14] Available online at http://www-bsac.eecs.berkeley.edu/~warneke/research/flicker.html

[15] Jammu, V.; Wang, K; Danai, K.; Lewicki, D. "Model-Based Sensor Location Selection for Helicopter Gearbox Monitoring"; NASA Technical Memorandum 107219 available through NASA Lewis Research Center or online at www.nasatech.com in the mechanics division.

Authorized licensed use limited to: Univ of Calif Berkeley. Downloaded on October 23,2022 at 23:26:37 UTC from IEEE Xplore. Restrictions apply.